Journal of Hydrology: Regional Studies 56 (2024) 101970

Contents lists available at ScienceDirect

Journal of Hydrology: Regional Studies

journal homepage: www.elsevier.com/locate/ejrh

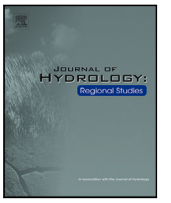

Sensitivity of montane grassland water fluxes to warming and elevated CO_2 from local to catchment scale: A case study from the Austrian Alps

Matevž Vremec [a,*], Peter Burek [b], Luca Guillaumot [b,c], Jesse Radolinski [d,e], Veronika Forstner [a,f], Markus Herndl [f], Christine Stumpp [g], Michael Bahn [d], Steffen Birk [a]

[a] Department of Earth Sciences, NAWI Graz Geocenter, University of Graz, 8010 Graz, Austria
[b] International Institute for Applied Systems Analysis, Laxenburg, Austria
[c] Water, Environment, Processes and Analyses Division, BRGM-French Geological Survey, Orleans, France
[d] Department of Ecology, University of Innsbruck, Innsbruck, Austria
[e] Department of Environmental Science and Technology, University of Maryland, College Park, MD, USA
[f] Institute of Plant Production and Cultural Landscape, Agricultural Research and Education Centre, Irdning-Donnersbachtal, Austria
[g] University of Natural Resources and Life Sciences, Vienna, Department of Water, Atmosphere and Environment, Institute of Soil Physics and Rural Water Management, Muthgasse 18, 1190 Vienna, Austria

ARTICLE INFO

Keywords:
Hydrologic response
Hydrological models
Climate change
Montane grassland
Lysimeter

ABSTRACT

Study region: Montane grassland within the Gulling catchment, Austrian Alps. Study focus: A climate-change experiment in a grassland ecosystem used lysimeters and HYDRUS-1D models to quantify changes in evapotranspiration (ET) and groundwater recharge (GWR) due to warming (+3 °C) and elevated CO_2 concentrations (ΔCO_2; +300 ppm). Findings at the plot-scale were generalized and transferred to the surrounding catchment, half comprised of grassland, using three lumped rainfall–runoff models and two spatially-distributed Community Water Models, differing in soil hydraulic properties.

New hydrological insights for the region: Warming increased ET and decreased GWR and river discharge compared to ambient conditions. ΔCO_2 increased stomatal resistance, which partially offset warming effects. In scenarios combining warming and ΔCO_2, the impact of warming was higher than ΔCO_2 effect. Elevation influenced the sensitivity of ET to warming, which was greater at the catchment scale than at the plot scale, while GWR was more sensitive to warming at the plot scale. Under dry conditions, GWR and discharge exhibited increased sensitivity to warming at both scales. HYDRUS-1D successfully reproduced lysimeter experiment results and their sensitivity to warming and ΔCO_2. Despite model agreement on water flux sensitivity to climate changes, the varying response magnitudes highlight the need for a multi-model approach in climate impact assessments. This study provides insights into how climate change might impact hydrological dynamics of montane grassland systems across the Central European Alps.

* Corresponding author.
E-mail address: matevz.vremec@uni-graz.at (M. Vremec).

https://doi.org/10.1016/j.ejrh.2024.101970
Received 27 June 2024; Received in revised form 3 September 2024; Accepted 5 September 2024
Available online 13 September 2024
2214-5818/© 2024 The Author(s). Published by Elsevier B.V. This is an open access article under the CC BY license (http://creativecommons.org/licenses/by/4.0/).

1. Introduction

Climate change is disrupting the hydrological cycle not only by altering precipitation patterns but also by increasing evaporative demand (IPCC, 2021; Allan et al., 2020; Teuling, 2018; Duethmann and Blöschl, 2018). Such changes may ultimately lead to reductions in both surface water and groundwater resources in various regions (Green et al., 2011; Haslinger et al., 2022). Further, recent work by Zhang et al. (2023) suggests that the sensitivity of river discharge to changes in evapotranspiration (ET) due to warming is greater than previously thought. Thus, understanding the impact of changing ET on water fluxes in a changing climate is critical for future assessments of water resources.

Rainfall–runoff models are commonly used to investigate how changes in precipitation and ET due to warming (denoted as ΔT) and elevated CO_2 concentrations (denoted as ΔCO_2) impact water fluxes at plot, regional, and global scale (Duethmann et al., 2020; Karlsson et al., 2016; Bastola et al., 2011; Broderick et al., 2016). Global-scale studies (Milly and Dunne, 2016; Berg et al., 2016; Zhang et al., 2023) have shown that the rise in terrestrial ET attributed to global warming often surpasses precipitation increases, resulting in continental drying. This phenomenon is largely driven by the direct effects of warming, which increase the vapor pressure deficit and the Clausius-Clapeyron slope, thereby increasing potential evapotranspiration (PET) (Scheff and Frierson, 2014; Milly and Dunne, 2016). In arid climates, the greening effect due to ΔCO_2 can further amplify the effects of ΔT, leading to higher water use for vegetation (Ukkola et al., 2016). Conversely, in humid regions with dense vegetation, ΔCO_2 can mitigate ΔT effects and contribute to water conservation through partial stomatal closure, a process by which plants close the openings on their leaves to regulate water loss (Leakey et al., 2009; Milly and Dunne, 2016; Ukkola et al., 2016; Yang et al., 2021). The contrasting or intensifying impacts of ΔT and ΔCO_2 on water fluxes are largely due to variations in regional climate and vegetation responses, highlighting the need for region-specific assessments of climate change impacts (Fatichi et al., 2016).

Prior research conducted in the Alpine region has predominantly focused on exploring the effects of climate change on water fluxes by analyzing historical river discharge observations (Duethmann and Blöschl, 2018; Duethmann et al., 2020) or employing hydrological models combined with regional climate change scenarios (Wagner et al., 2017; Hanus et al., 2021). These studies commonly report that warming leads to a decrease in overall river discharge and an increase in ET, especially in summer. However, these findings were mainly derived from individual modeling exercises and offer limited insight into the sensitivity of specific water fluxes at different scales or across different models. Several studies have demonstrated that the choice of the hydrological model can affect the simulated response of groundwater recharge and river discharge to climate change (Moeck et al., 2016; Karlsson et al., 2016; Broderick et al., 2016). This underscores the importance of empirical data to support these results and the importance of a multi-model approach to better constrain the impact of ΔT and ΔCO_2 on water fluxes (Fatichi et al., 2016).

To address this knowledge gap, a long-term climate-change experiment was conducted in a montane grassland in the Austrian Alps (Piepho et al., 2017; Herndl et al., 2011), a region where grassland ecosystems cover about 40%–45% of the land area and play a central role in regulating the water balance (BMLRT, 2020; Inauen et al., 2013; Wieser et al., 2008). Data from this experiment, analyzed by Forstner et al. (2021) for the period 2015–2018, was derived from six high-precision weighing lysimeters operated under conditions of increased temperature and elevated CO_2 concentrations. The study found that warming (+3 °C) led to an increase in ET and a decrease in groundwater recharge, while ΔCO_2 (+300 ppm) had the opposite effect, leading to a decrease in ET and increase in groundwater recharge. These effects are attributed to the reduction in plant transpiration due to partial stomatal closure from CO_2 enrichment (Vremec et al., 2023; Leakey et al., 2009). However, when both ΔT and ΔCO_2 were present, the ΔCO_2 effect did not fully counterbalance the increased ET caused by ΔT, resulting in a net increase in ET compared to current ambient climatic conditions.

In this study, we expand our understanding of how climate change affects the hydrological cycle, by moving beyond plot-scale investigations of montane grasslands water fluxes (lysimeter experiments and HYDRUS-1D models) to a catchment scale analysis utilizing five rainfall–runoff models. This includes three lumped-parameter models (GR4J, HyMod, and HBV_{EDU}) and two spatially-distributed Community Water Model (CWatM) models. Specifically, we evaluate

- how changes in PET, driven by ΔT and ΔCO_2, impact the water fluxes observed at plot scale and to which extent these observations can be reproduced by soil hydrological modeling;
- how and why the impacts of changes in PET on modeled water fluxes differ from the plot scale to the catchment scale;
- how the simulated impacts at catchment scale vary across different rainfall–runoff models.

This multi-model approach is aimed to underscore the broader implications and to address the uncertainties associated with upscaling the climate-driven changes of water fluxes through various models.

2. Data and methods

2.1. Study site

The investigated area was the Gulling catchment, located in the Enns valley of Austria, adjacent to the experimental facility shown in Fig. 1. The catchment spans an area of 156 km^2 and covers an altitude range from 644 to 2220 m, with a mean elevation of 1430 m. Half of the catchment comprises grassland (51%; mainly including pastures, alpine meadows, and extensive and managed grassland), 48% is forested, while the remaining 1% consists of high elevation bare rock surfaces and water bodies. The soil in the catchment is mainly composed of cambisol (62%), podzol (35%), and luvisol (3%). The catchment receives an average annual

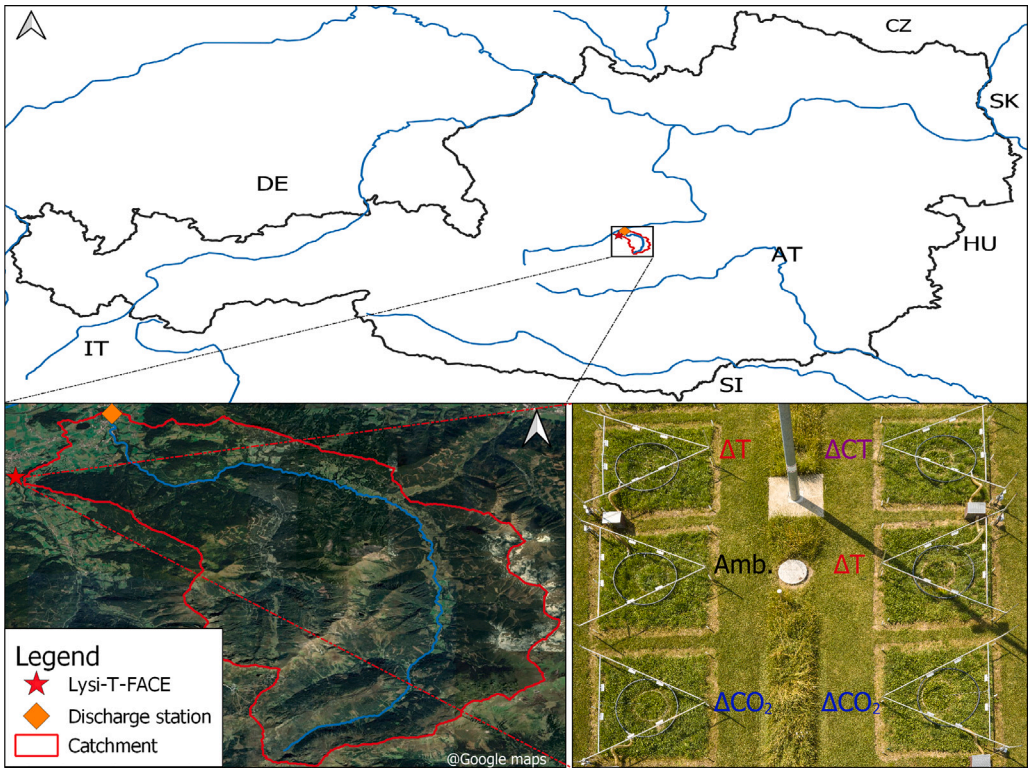

Fig. 1. Location of the Gulling catchment and the Lysi-T-FACE experimental site with their different factor combinations: ambient (Amb.), +3 °C (ΔT), +300 ppm CO_2 (ΔCO_2), and +3 °C combined with +300 ppm CO_2 (ΔCT).

precipitation of 1450 mm (1990–2016), is influenced by snowmelt during spring, and has an average annual temperature of 5.2 °C (1990–2016).

The main experimental plot site was the Lysi-T-FACE experiment conducted at the AREC Raumberg-Gumpenstein research station (Piepho et al., 2017; Herndl et al., 2011). The objective of this climate-change experiment was to investigate the effects of ΔT, ΔCO_2, and drought on the ecohydrology of managed montane grassland. The facility is situated at an elevation of 707 m above sea level, close to the confluence of the Enns and Donnersbach rivers in the eastern Austrian Alps. Among the plant communities present are grasses such as *Arrenatherum elatius* and *Festuca pratensis*, and legumes such as *Lotus corniculatus* and *Trifolium pratense*, which are typical of permanent grassland in the Alps (Schaumberger, 2011). Preliminary analysis revealed three soil horizons at the site (A_{ph}: 0–25 cm, B_v; 26–90 cm, C_v: > 100 cm), with the soil type classified as a Cambisol, primarily consisting of loamy sand with soil texture analyzed according to ÖNORM L 1050 for the A (45 ± 5% sand, 45 ± 5% silt, and 9 ± 3% clay) and B horizon (53 ± 10% sand, 37 ± 8% silt, and 10 ± 3% clay). The median bulk density of the upper two horizons is 1.4 g cm^{-1}, and the median saturated hydraulic conductivity is 114 cm day (range: 50.5–234.1 cm day^{-1}). The average annual precipitation at the site is 1077 mm (1991–2020) with an annual mean temperature of 8.5 °C (1991–2020).

2.2. Workflow

Our approach to assess the individual and combined effects of ΔT and ΔCO_2 on the sensitivity of potential evapotranspiration (PET), and in turn on actual evapotranspiration, groundwater recharge, and river discharge at both the plot and catchment scales, consisted of three main steps (Fig. 2):

1. Quantification of the effects of ΔT and ΔCO_2 at the plot scale using lysimeter soil water fluxes.
2. Generalization of plot-scale findings to compute PET for different levels of ΔT and ΔCO_2, cross-checking the results with lysimeter data.
3. Simulation of three climate change scenarios at the plot and catchment level, mirroring the lysimeter experiment, to compare water flux changes against current ambient climatic conditions.

Each step followed a *storyline* approach (Shepherd, 2019; Buitink et al., 2021), where the current or past hydrological system was influenced by future conditions (ΔT and ΔCO_2). Such approaches have been used to better understand (a) process changes and (b) system response to changes in climate conditions (Van Tiel et al., 2023). We explain each step in more detail below. The first two

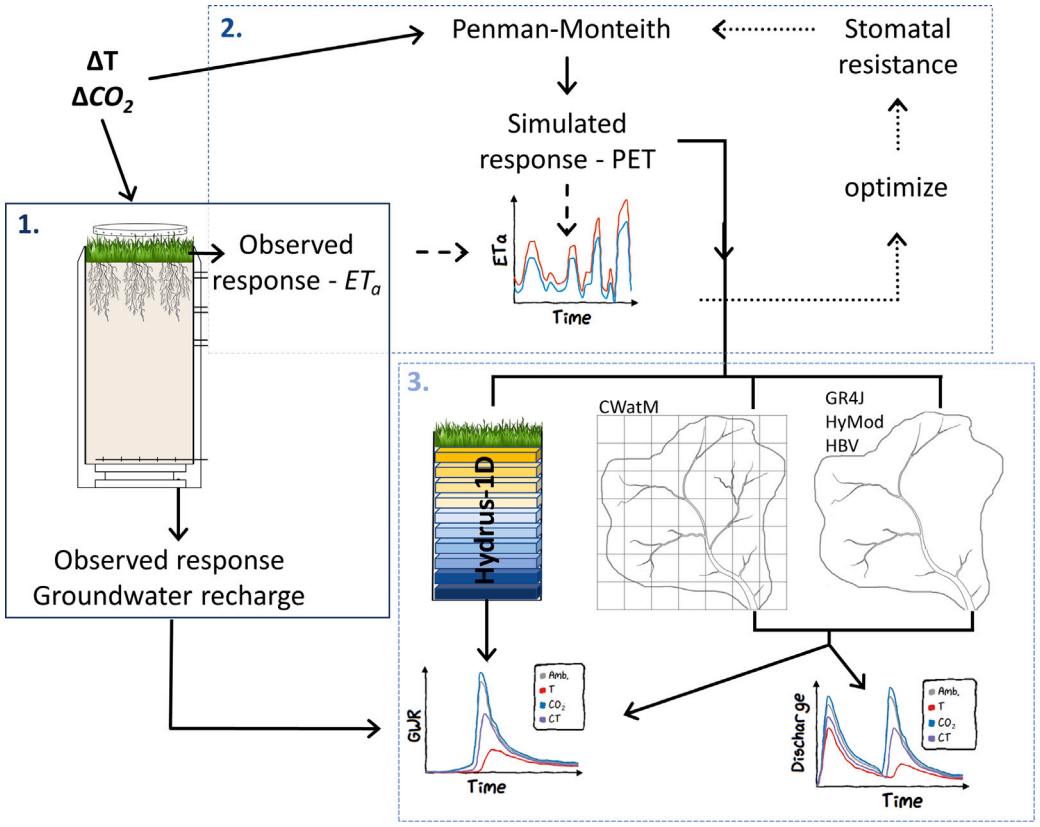

Fig. 2. Schematic representation of the study's workflow, which involved: (1) quantifying responses of lysimeter soil water fluxes to warming (ΔT) and elevated CO_2 concentrations (ΔCO_2); (2) generalizing the findings from lysimeter experiments; and (3) upscaling these results to the catchment level.

steps covered the lysimeter observation period from 2016 to 2021, while the last step covered the years 1990 to 2016 to account for local climate variability and enable comparisons at both plot and catchment levels.

2.3. Lysimeter soil water fluxes

In the study, lysimeters were used to quantify the components of the soil water balance, comprising precipitation (P), actual evapotranspiration (ET_a), groundwater recharge (GWR) and the change in the soil water storage ΔS, assuming no overland flow occurred:

$$\Delta S = P - ET_a - GWR \tag{1}$$

Data from six high-precision weighing lysimeters, which are part of the Lysi-T-FACE concept that applies a heating treatment and free-air controlled enrichment with CO_2 to open-field plant canopies (Herndl et al., 2011), were used to quantify and generalize the effects of ΔT and ΔCO_2. Here, the dataset from Forstner et al. (2021) formed the basis for our analysis, which we then extended by expanding the observation period for three more years. The six lysimeters were divided into different treatments: two were treated with ΔCO_2, two with ΔT, one with both ΔCO_2 and ΔT, and one remained under ambient conditions. To achieve a controlled increase of +300 ppm in CO_2 compared to ambient conditions, the ΔCO_2-treated lysimeters were subjected to a Free Air Carbon dioxide Enrichment (FACE) system as described by Miglietta et al. (2001). Temperature control was accomplished using an infrared heater-based free air enrichment system (T-FACE) to raise the temperature by +3 °C (relative to ambient surface temperature), following the method outlined by Kimball (2005). Daily soil water fluxes were calculated by resampling 10-min water balance data to daily sums. Leaf area index (LAI) measurements were conducted throughout the growing season using the AccuPAR LP-80 Ceptometer, with at least 10 measurements per year per lysimeter. A more detailed description of the lysimeter setup can be found in Herndl et al. (2011) and Forstner et al. (2021), as well as in the Supplementary material. We quantified changes in annual lysimeter soil water fluxes for the growing season from 2016 to 2021, a period which included the relatively dry years of 2018 and 2019. The start and end of each growing season were defined based on the thermal approach of Ernst and Loeper (1976), computed using daily average ambient temperature (see Supplementary material). To evaluate the significant effects of ΔT and ΔCO_2 on daily actual evapotranspiration, groundwater recharge, and LAI measurements from the lysimeters, we employed an analysis of variance

(ANOVA) followed by a post hoc Tukey test. We limited our daily ET_a analysis to days when the CO_2 concentration in CO_2–enriched lysimeters was within 30% of the target (+300 ppm) and the ΔT lysimeters were within 30% of the target temperature increase (+3 °C) (0.7 < TAR < 1.3; TAR = target achievement ratio).

2.4. Potential evapotranspiration under ΔT and ΔCO_2

Potential evapotranspiration for the lysimeter treatments, the plot and catchment scale hydrological models, was computed using the Penman–Monteith (PM) equation (Allen et al., 1998):

$$PET = \frac{1}{\lambda}\left[\frac{\Delta(R_n - G) + \rho_a c_p k(e_s - e_a)/r_a}{\Delta + \gamma(1 + \frac{r_s}{r_a})}\right] \quad (2)$$

where PET is the potential evapotranspiration [kg m^{-2} d^{-1} equivalent to mm d^{-1}], λ is the latent heat of vaporization [MJ kg^{-1}], Δ is the slope of the saturation vapor pressure curve [kPa K^{-1}], R_n [MJ m^{-2} d^{-1}] is the net radiation, G is the soil heat flux [MJ m^{-2} d^{-1}], ρ_a is the air density [kg m^{-3}], c_p is the specific heat of dry air [MJ kg^{-1} K^{-1}], e_s is the saturation and e_a is the actual vapor pressure of the air [kPa], γ is the psychrometric constant [kPa K^{-1}], r_s is the bulk surface resistance [s m^{-1}], r_a is the bulk aerodynamic resistance [s m^{-1}], and k is for unit conversion (=86 400) [s d^{-1}]. The value of r_a was calculated using crop height (equation 4 in Allen et al., 1998), with an assumed value of 0.12 LAI following Vremec et al. (2021). Net radiation was computed as incoming net shortwave radiation minus outgoing net longwave radiation, according to equation 40 in Allen et al. (1998). This calculation used measured solar radiation and daily mean, maximum, and minimum temperatures. G was set to 0 as suggested by Allen et al. (1998).

The PM equation was combined with an adapted CO_2-dependent stomatal resistance model to capture the effect of ΔCO_2 on stomatal resistance and LAI (Yang et al., 2019; Vremec et al., 2023, 2024):

$$r_s = \frac{r_l(CO_2)}{LAI} = \frac{r_{r_l-300} \times \left\{1 + S_{r_{l-CO_2}} \times ([CO_2] - 300)\right\}}{LAI} \quad (3)$$

where $S_{r_l-[CO_2]}$ [ppm^{-1}] is the relative sensitivity of r_l to $\Delta[CO_2]$; and r_{r_l-300} [s m^{-1}] is the reference stomatal resistance when atmospheric $[CO_2]$ is 300 ppm. The relative sensitivity of r_l to $\Delta[CO_2]$ represents the change in r_l per ppm increase in $[CO_2]$.

We used the two equations above to (i) assess changes in stomatal resistance under ΔCO_2 by inversely estimating stomatal resistance at lysimeters with ambient CO_2 and lysimeters treated under ΔCO_2, and (ii) obtain r_{r_l-300} and $S_{r_{l-CO_2}}$, which are necessary to compute PET at any CO_2 concentration. Here, r_{r_l-300} and $S_{r_{l-CO_2}}$ were estimated by comparing calculated PET (using the PM equation) with the measurements obtained from lysimeters. To estimate these parameters, the trust-region reflective least squares algorithm, as implemented in Scipy (Virtanen et al., 2020), was employed. This analysis was conducted only on days when the ET_a measured by the lysimeter was considered equivalent to the PET demand. The relevant periods were identified according to Vremec et al. (2023), selecting days when plant transpiration was not limited by water availability and the LAI was greater than 2. The periods when water availability affected plant transpiration were defined as days when the soil moisture anomaly index (calculated from the soil water content at a depth of 30 cm) was below –2. This procedure was performed for all six lysimeters, where approximately 50% of the data was preserved.

Experimental warming of grassland can impact the vapor pressure deficit (VPD) between the inside of the leaves and the outside air, under conditions of (i) constant relative humidity (RH = constant) or (ii) constant actual vapor pressure (e_a = constant) (Kimball, 2005; Scheff and Frierson, 2014):

$$VPD = e_s(1 - RH) = e_s - e_a, \quad (4)$$

where RH is the near-surface relative humidity. In scenarios where e_a is constant, RH would have to decrease. Scheff and Frierson (2014) recommend examining the impact of global warming on PET under constant RH to observe how variations in e_s influence VPD and PET. However, to better represent the open-field conditions of our infrared-heated plot, where warming was not performed everywhere (i.e. by global warming), we adapted our model to evaluate the effects on PET under constant e_a conditions, following Kimball (2005). Recent insights from land surface observations (Douville and Willett, 2023) suggest that such scenarios may indeed reflect real-world conditions over land to some extent, where relative humidity is expected to decrease (Allan et al., 2020). As such, PET was estimated using the Penman–Monteith equation, adjusting the ambient daily temperature by the ΔT factor for computing e_s, Δ, and ρ_a, thereby increasing VPD and the Clausius-Clapeyron slope, while keeping other variables constant (R_n, e_a, r_a, r_s γ, λ, c_p). This approach was also applied at the catchment to enable a direct comparison between the different scales. The effects of ΔT on PET under constant RH are also presented in Supplementary material, Figure S8.

The daily meteorological data used to estimate PET were obtained from on-site meteorological, including temperature, wind speed, relative humidity, and solar radiation. LAI data from 2016 to 2021 were derived from AccuPar measurements, while a mean LAI of 2.2, representing the growing season average, was applied to the period from 1990 to 2016. Model performance was analyzed using the Kling-Gupta efficiency (KGE), and the bias was calculated as the mean of the differences between observed and simulated values.

2.5. Plot-scale hydrological model

Soil water fluxes at the plot scale were modeled with a HYDRUS-1D model (Šimůnek et al., 2008). This model takes PET as input, and divides it into potential soil evaporation and potential transpiration using Beer's law (Ritchie, 1972). The model then calculates actual transpiration and groundwater recharge based on the availability of water in the root zone, as described by Van Genuchten (1980). The soil water retention and hydraulic conductivity function were characterized using the unimodal Van Genuchten–Mualemmodel (Van Genuchten, 1980). The soil horizon was divided into three layers, each layer represented by a set of soil hydraulic properties. The meteorological data used for estimating PET, along with the daily precipitation data that served as input for the HYDRUS-1D model, were acquired from the onsite Irdning station (approximately 150 m from the study site), operated by the national meteorological service GeoSphere Austria. PET was estimated according to Section 2.4.

The calibration of the HYDRUS-1D model was performed using daily seepage rates at the lower lysimeter boundary, soil water content, and matric potential data obtained from the ambient weighing lysimeter at a depth of 10 and 30 cm. Given that soil water content rarely reached very dry conditions near the wilting point, we complemented our calibration data with matric potential and soil water content data collected in the drier range (see Supplementary material, Figure S1). This additional dataset was obtained with the WP4C dew point potentiometer from disturbed soil samples. We incorporated this additional dataset to improve the predictive capability, particularly under drier conditions. To capture the effects of both wet and dry years, the entire available period (2016–2021) was used for calibration (Shen et al., 2022). During this period, annual precipitation ranged from 946 mm in 2021 to 1275 mm in 2017, and average annual temperatures varied from 7.9 °C in 2021 to 9.1 °C in 2018.

The DREAM$_{ZS}$ (DiffeRential Evolution Adaptive Metropolis) global optimization algorithm, as implemented in the Spotpy package (Houska et al., 2015) and described by Vrugt (2016), was employed to calibrate the HYDRUS-1D model. With a range of different measurement types for the HYDRUS-1D model, the data likelihood was aggregated as the sum of the logarithmic likelihoods of each measurement type following Schübl et al. (2022). We constrained the uniform prior distributions using physically plausible values derived from previous modeling studies at the site (Stumpp et al., 2012; Schübl et al., 2022) and laboratory soil analyses, while the standard deviations of the measurement errors were determined using data from the duplicated lysimeters. For more details on the calibration procedure, see Supplementary material.

We undertook the plot-scale modeling exercise for two key reasons. The first was to compare the observed sensitivity of water fluxes, based on lysimeter data, to those predicted by our simulations at the plot scale (2016–2021). The second was to obtain plot-scale water flux data for the period 1990–2016, enabling a comparison of water fluxes at plot and catchment scale within the same timeframe.

2.5.1. Catchment rainfall–runoff models

In this catchment modeling study, we selected a range of widely applied hydrological models, each with varying complexity and distinct methodologies for representing soil and water routing processes. The spatially-distributed Community Water Model (CWatM) model was chosen for its physically-based representation of hydrological processes, including infiltration, evapotranspiration, groundwater recharge, and snow melt, and its wide application in regional and global scale studies. The non-linear soil moisture accounting module of CWatM simulates unsaturated zone flow using the Richards equation with the Van Genuchten simplification (Van Genuchten, 1980). The lumped parameter models–GR4J (Perrin et al., 2003), HyMod (Moore, 1985), and HBV$_{EDU}$ (Aghakouchak and Habib, 2010)–were selected for their simple structure, the same input data requirement, small number of model parameters (<8), and their common use in climate change impact studies focusing on river discharge.

Two CWatM models (Burek et al., 2020) were used, which required information on landcover and soil hydraulic properties. These two models differed in the used soil hydraulic properties: one model used data from the Harmonized World Soil Database 1.2. (referred to as CWatM C model), while the other used the same soil hydraulic properties as the HYDRUS-1D model (referred to as CWatM $C*$ model) (see Supplementary material, Figure S4). The lumped-parameter models and the CWatM model utilized data with a daily temporal resolution. Additionally, the CWatM model employed a spatial resolution of 1×1 km^2. A more detailed description of the models is available in the Supplementary material.

Meteorological data (including precipitation, temperature, wind, relative humidity, and solar radiation) for the Gulling catchment was obtained from the Spartacus dataset in the form of 1×1 km gridded datasets for the period between 1990–2016 (Hiebl and Frei, 2016, 2018). Discharge data for the Gulling river was collected from the Aigen station, which is operated and made available by the Central Hydrographical Bureau (HZB; https://ehyd.gv.at/, last access: 17 March 2023). The land cover information was obtained from the EU CORINE Land Cover (2018) and the soil map from the Harmonized World Soil Database 1.2.

The catchment-scale modeling workflow consisted of the following steps:

1. Calibration of CWatM using historical climate and discharge data.
2. Calibration of the lumped-parameter models, utilizing catchment averaged PET, rainfall, and snowmelt (from CWatM) along with discharge data.
3. Adjustment of PET to reflect different ΔT and ΔCO_2 scenarios.
4. Execution of climate change scenarios across all models.

Our main focus in employing the rainfall–runoff models was to determine how changes in PET affect water fluxes at the catchment scale and to understand how model choice and complexity influence the sensitivity of these fluxes to changes in PET. Thus, to improve comparability between models, we utilized the same catchment averaged rainfall, snowmelt and PET values computed by the CWatM model for all the rainfall–runoff models. As the catchment consisted of approximately 50% grassland and 50%

forest, we computed PET for each landcover type as follows. For grassland areas, PET in the CWatM model was calculated using the Penman–Monteith equation with stomatal resistance values calibrated from Section 2.4. For forest and other land cover types, we used the FAO-56 Penman–Monteith equation for a well-watered grass reference crop (Allen et al., 1998). Given the current understanding about the sensitivity of ET of spruce and pine forests (Ward et al., 2018), which are the dominant forest type in the catchment, to elevated CO_2 concentrations, we assumed forest areas to be non-sensitive to elevated CO_2. Finally, to generate an average PET value for each grid cell in the CWatM model, we multiplied the estimated PET for grassland or non-grassland areas by the corresponding land cover fraction from the CORINE Land Cover map. For the analysis at the catchment level, we assumed an LAI of 2.2 for grassland, which is consistent with the calculations at the plot level.

Calibration followed a split-sample approach: the first seven years were allocated for the warm-up period, the next ten years (1997–2006) for validation, and the last ten years (2007–2016) for calibration. The CWatM calibration employs the DEAP framework in Python (Fortin et al., 2012), implementing the NSGA-II evolutionary algorithm (Deb et al., 2002). We used a modified Kling-Gupta efficiency (KGE) metric defined by Kling et al. (2012) and implemented in CWatM (Burek et al., 2020). Additionally, the lumped-parameter models were calibrated using the DREAM algorithm (Vrugt, 2016), which is compatible with a modified KGE metric by Liu et al. (2022). This choice was due to the metric's compatibility with the Bayesian framework used in DREAM. The rainfall–runoff models' calibration was based on daily discharge. The performance of the rainfall–runoff models was analyzed by employing the KGE for overall and high flows and log-transformed KGE (logKGE) for low flow performance (Gauch et al., 2023).

2.5.2. Analysis of change of the modeled climate change scenarios

Using one plot and 5 different rainfall–runoff models, we simulated three climate change scenarios reflecting the lysimeter treatments and corresponding to the RCP 6.0 scenario (see Supplementary material, Figure S5; Van Vuuren et al., 2011):

1. warming of 3 °C (ΔT scenario);
2. an increase in CO_2 concentration of 300 ppm (ΔCO_2 scenario);
3. warming of 3 °C combined with an increase in CO_2 concentration of 300 ppm (ΔCT scenario)

The relative sensitivity of water fluxes to ΔT and ΔCO_2, was represented as relative changes between the climate change scenarios water flux and the ambient conditions. In these scenarios, only the input PET was altered, with precipitation unchanged. At the catchment scale, we assessed the effects on ET_a, GWR, and river discharge. Since each rainfall–runoff model includes a different soil storage component, percolation was calculated internally as the water exiting the soil storage. Given that our calculations included annual fluxes, we assumed all percolation to eventually contribute to groundwater recharge. To account for local climate variability and to compare plot and catchment models, all models used meteorological data from 1990 to 2016.

The ΔCT scenario, being the most realistic rather than purely mechanistic, was employed in a detailed examination of its impacts on river discharge (Q), focusing on high (95th percentile, $\Delta Q95$) and low flows (5th percentile, $\Delta Q5$). Additionally, their relationship with the aridity index (AI), computed as annual precipitation divided with PET, was assessed.

3. Results

3.1. Observed changes in lysimeter water fluxes

The lysimeter water fluxes, shown in Fig. 3, revealed distinct effects of ΔCO_2 and ΔT. Specifically, ΔCO_2 led to a general decrease in actual evapotranspiration (ET_a) by –6 ± 4% and an increase in groundwater recharge (GWR) by 17 ± 17% from 2016 to 2021. In contrast, ΔT resulted in an increase in ET_a by 17 ± 8% and a decrease in GWR by –47 ± 19%. When both ΔT and ΔCO_2 were present (ΔCT), the influence of ΔT prevailed against ΔCO_2, causing an increase in ET_a by 9 ± 9% and a decrease in GWR by –40 ± 18%. Notably, both ΔT and ΔCT were associated with reduced precipitation, primarily due to a decline in non-rainfall water (dew and fog) by –5 ± 2%, while ΔCO_2 slightly increased precipitation by 2 ± 4%. Changes in non-rainfall due to ΔT and ΔCO_2 are explained in greater detail in Forstner et al. (2023). Changes in soil water storage during the growing season (ΔS), were most pronounced due to ΔT in 2018, followed by 2019 and 2020 (Fig. 3d). The ΔT lysimeters showed the largest changes in ΔS, contrasting with minimal changes in the ΔCO_2 lysimeters, which exhibited the smallest differences in ΔS. These observations are consistent with Forstner et al. (2021), who analyzed the same dataset for the period 2015–2018.

ANOVA and post-hoc Tukey tests conducted on daily ET_a and GWR showed significant differences ($p < 0.05$) among the groups (Ambient [Amb], ΔCO_2, ΔCT, ΔT), except for the comparison between ΔCT and the ambient lysimeter. Interestingly, when the dry years of 2018 and 2019 were excluded from the ANOVA analysis, a significant difference emerged between these two groups as well.

3.2. Implication of the ΔT and ΔCO_2 effects in the Penman-Monteith equation

When comparing ET_a measurements from lysimeters, under non-water-limited conditions, to estimates derived with the Penman–Monteith equation, we found that lysimeters treated with elevated CO_2 exhibited higher stomatal resistance values (103 ± 14 s m^{-1}), compared to those without CO_2 treatment (71 ± 14 s m^{-1}) (Fig. 4,c). To generalize these findings and compute PET at any CO_2 concentration, we calibrated the CO_2-adjusted stomatal resistance model, as per Eq. (3). The calibrated values were 65 ± 7 s m^{-1} for the reference stomatal resistance at 300 ppm and 0.002 ppm^{-1} for the relative sensitivity of stomatal resistance to CO_2. The ANOVA analysis on the measured LAI data from 2016 to 2021 indicated no significant effects (Fig. 4,b) of ΔT or ΔCO_2 on LAI,

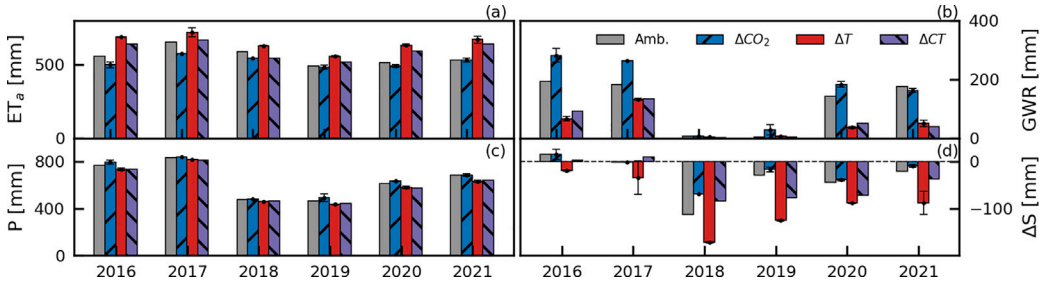

Fig. 3. Absolute values of actual evapotranspiration (ET$_a$; **a**), groundwater recharge (GWR; **b**), precipitation (P; **c**), and the change in soil water storage (ΔS; **d**) for each of the growing seasons from 2016 to 2021.

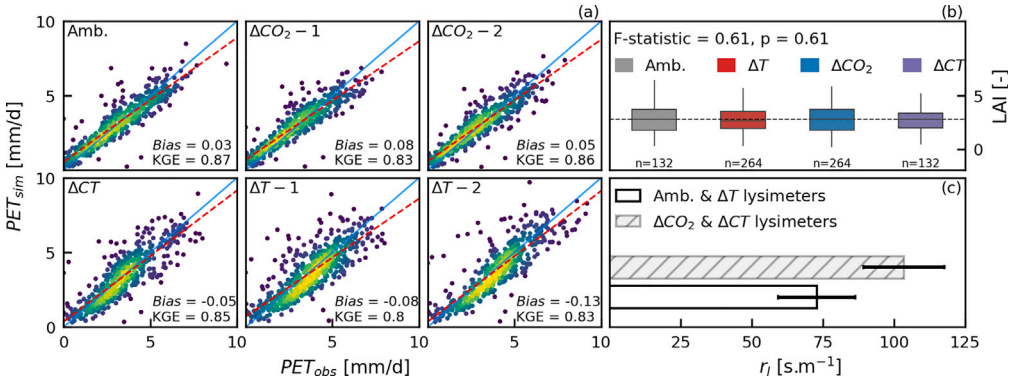

Fig. 4. Scatterplots comparing the potential evapotranspiration observed at the lysimesters (PET$_{obs}$) with the estimated PET using the adapted Penman–Monteith equation (PET$_{sim}$; **a**). The box plots display the leaf area index (LAI) for each treatment, including ANOVA results (**b**). The estimated stomatal resistance obtained from inverse modeling for lysimeters under ambient CO_2 and ΔCO_2 conditions is presented as a bar plot in panel (**c**).

suggesting that the changes in ET due to ΔCO_2 were primarily driven by stomatal resistance change. We then applied the CO_2-adjusted Penman–Monteith equation, with estimated stomatal resistance and sensitivity specific to our grassland site, to validate estimated PET for each lysimeter. The model performance was robust for all lysimeters, as indicated by KGE higher than 0.8 and minimal model biases (Fig. 4,a).

3.3. Observed versus modeled changes in water fluxes due to ΔT and ΔCO_2 at the plot scale

The calibrated HYDRUS-1D model showed good performance in simulating the water fluxes of the ambient lysimeter, as indicated by a KGE of 0.83 for groundwater recharge and a KGE higher than 0.75 for soil water content (see Supplementary material, Figures S1-S3). Fig. 5 presents the model's sensitivity to ΔT and ΔCO_2, illustrating relative changes in annual water fluxes between the climate change scenarios and ambient conditions for both modeled data (HYDRUS-1D; 1997–2016) and observed data (lysimeters; 2016–2021). Despite covering different periods, the modeled water fluxes exhibited similar mean annual sensitivity to ΔT and ΔCO_2 as the lysimeters; though the lysimeter data showed greater annual variability (Fig. 5).

For ΔCO_2, sensitivities of simulated and observed PET were –6 ± 0.5% and –6 ± 5%, respectively. Under ΔT, they were 17 ± 2% for simulated and 18 ± 8% for observed PET. For ΔCT, the sensitivities were 10 ± 1% in the simulated data and 10 ± 10% in the observed data. Similarly, the sensitivities of both simulated and observed actual evapotranspiration (ET$_a$) to ΔCO_2 were –6 ± 0.5% and –5 ± 5%, to ΔT were 16 ± 2% and 17 ± 8%, and to ΔCT were 10 ± 1% and 9 ± 10%. Lastly, the sensitivities of GWR to these changes were 12 ± 6% and 8 ± 11% for ΔCO_2, –31 ± 10% and –28 ± 19% for ΔT, and –19 ± 1% and –25 ± 20% for ΔCT.

3.4. Modeled changes in water fluxes at the catchment scale

3.4.1. Performance of the rainfall–runoff models to simulate river discharge

Performance metrics for both the calibration (KGE$_{cal}$, 2007–2016) and validation period (KGE$_{val}$, 1997–2006) indicated strong model performance, with KGE values exceeding 0.8 (Table 1). Notably, the CWatM and GR4J models performed particularly well in capturing low flows, indicating their robustness in varied flow conditions, while the HBV and Hymod models were less effective in capturing low flow dynamics.

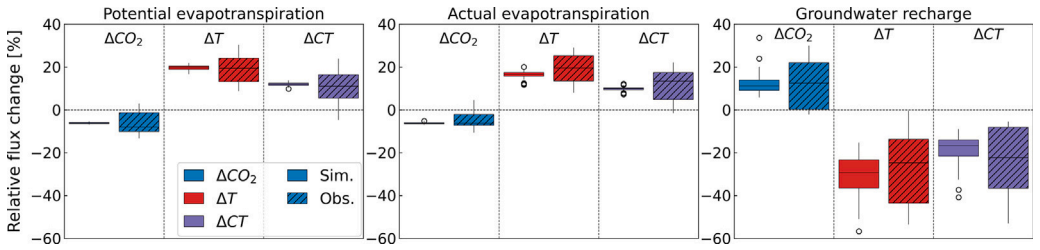

Fig. 5. Annual observed and modeled relative changes in potential evapotranspiration, actual evapotranspiration, and groundwater recharge at the plot scale. The box plots show the annual variability in the relative change of the water flux between the climate change scenario and ambient conditions, for observed fluxes between 2016–2021 and modeled fluxes between 1997–2016.

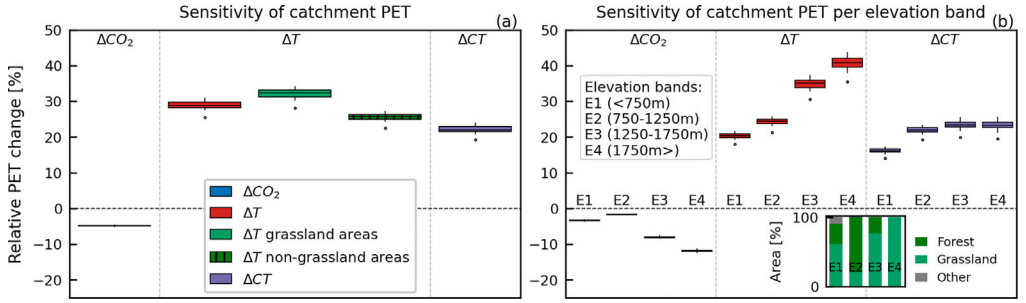

Fig. 6. Box plots illustrating the annual relative change in estimated catchment-averaged PET between the climate change scenarios and ambient conditions (**a**), and the relative average catchment PET change per elevation band within the catchment for these same scenarios (**b**).

Table 1
Kling-Gupta efficiency (KGE) and KGE in logarithmic space (logKGE) for all rainfall–runoff models. CWatM (C) model used soil hydraulic properties from the Harmonized World Soil Database 1.2, while CWatM (C*) used soil hydraulic properties obtained from the ambient lysimeter.

Model	KGE_{cal}	KGE_{val}	$logKGE_{cal}$	$logKGE_{val}$
GR4J	0.85	0.80	0.85	0.79
HBV_{EDU}	0.85	0.83	0.73	0.60
HyMod	0.84	0.83	0.45	0.4
CWatM (C)	0.80	0.84	0.75	0.81
CWatM* (C*)	0.80	0.82	0.68	0.75

3.4.2. Potential evapotranspiration

The analysis demonstrated that annual catchment-scale PET was influenced by both ΔT and ΔCO_2 during the modeled period from 1997 to 2016 (Fig. 6). ΔT led to an increase in annual PET of 30 ± 1% compared to ambient conditions, while ΔCO_2 resulted in a reduction of –5 ± 0.1%. Under the ΔCT scenario, there was a mean increase in PET of about 23 ± 1%. As detailed in Section 2.4, evapotranspiration for the catchment was calculated separately for grassland and non-grassland areas, with each grid cell's results aggregated according to their respective landcover fractions. Notably, the estimated PET for grassland areas showed greater sensitivity to ΔT (32 ± 1%) compared to the FAO-56 equation (27 ± 1%) used for non-grassland areas. Additionally, we found that its sensitivity to both ΔT and ΔCO_2 intensifies with increasing elevation. This trend was further clarified through a simple sensitivity analysis presented in Figure S6 in the Supplementary material. The analysis reveals that PET becomes more sensitive to increases in ΔT under conditions of lower temperatures and higher wind speeds, which are typical at higher altitudes.

3.4.3. Impact on actual ET, groundwater recharge and river discharge

The results of the catchment-scale modeling show that ΔT increases ET_a and decreases GWR and discharge across all models, while ΔCO_2 has the opposite minor effect (Fig. 7). These models consistently showed the same direction of sensitivity for all fluxes: a mean change in ET_a of –4 ± 1% for ΔCO_2, 24 ± 4% under ΔT, and 19 ± 3% for ΔCT. Similarly, GWR and discharge sensitivities were closely aligned, with increases of 2 ± 1% under ΔCO_2 and decreases of –12 ± 3% under ΔT and –10 ± 3% for ΔCT for GWR. Discharge sensitivity to ΔCO_2 was 2 ± 0.4%, –11 ± 2% under ΔT, and –9 ± 2% for ΔCT.

While the direction of change was consistent across all models, the magnitude of relative sensitivity varied, particularly under the ΔT and ΔCT scenarios. Notable inter-model differences were observed, especially for the ET*a* flux under ΔT, with the HBV_{EDU} and CWatM models showing mean relative changes of 20 ± 1% and 28 ± 2%, respectively. In the ΔCT scenario, the GR4J model exhibited the greatest decrease in river discharge, whereas the HBV_{EDU} model showed the least decrease. The GR4J model demonstrated the

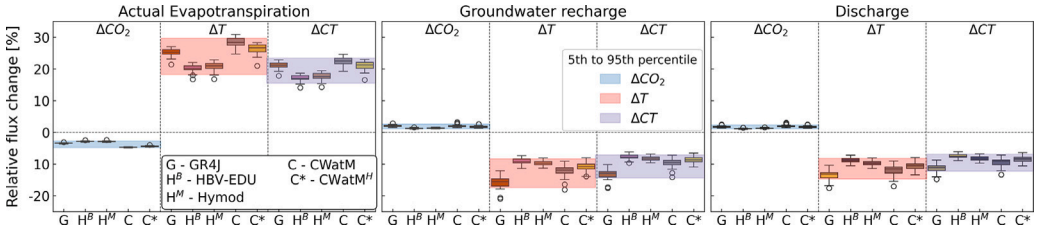

Fig. 7. Modeled relative changes in actual evapotranspiration, groundwater recharge and discharge for GR4J (G), HBV_{EDU} (H^B), HyMod (H^M), CWatM (C), and CWatM* (C*) models. The box plots show the annual variability in the relative change of the flux under the climate scenario and ambient conditions, while the uncertainty bands in each figure represent the 5%–95% range of annual variability in the simulated water flux.

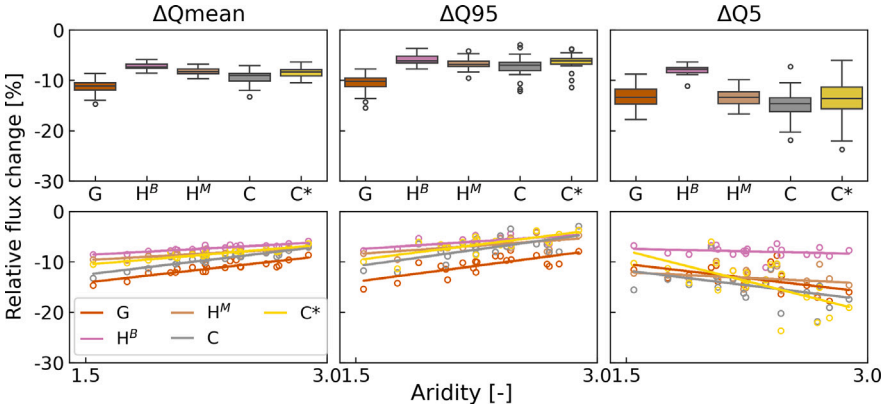

Fig. 8. The upper panels show the relative difference of mean ($\Delta Qmean$), high ($\Delta Q95$) and low ($\Delta Q5$) flows between the ΔCT and the ambient scenario at the catchment scale for GR4J (G), HBV_{EDU} (H^B), HyMod (H^M), CWatM (C), and CWatM* (C*) models. The lower panels of the figure show how the relative change in the flows correlates with the annual aridity index.

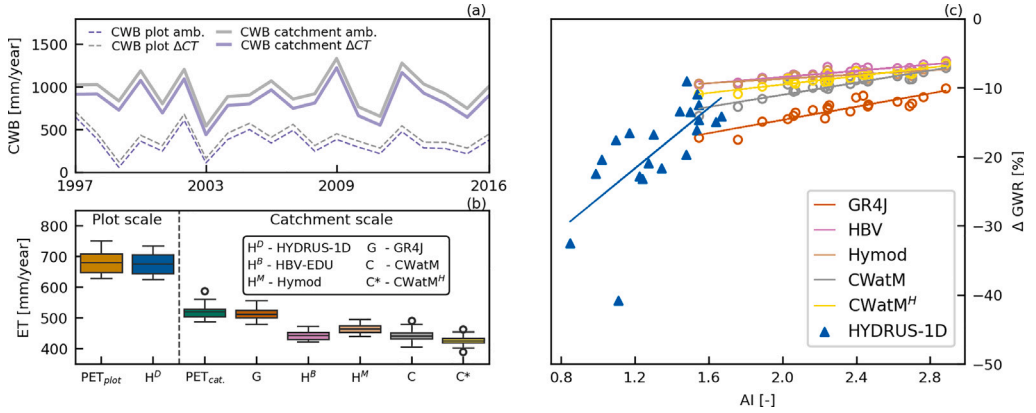

Fig. 9. The calculated annual climatic water balance for the ambient and ΔCT scenario (**a**), the modeled annual PET and ET_a for the plot and catchment scale (**b**), the relative change of GWR between ambient conditions and ΔCT scenario in relation to aridity for the plot scale, with HYDRUS-1D simulated GWR serving as proxy for lysimeter observations, and at the catchment scale (**c**).

highest sensitivity in annual river discharge, with a mean relative change of –13 ± 2%, contrasting with the HBV_{EDU} model, which had the smallest deviation at –9 ± 1

3.4.4. Sensitivity of extreme flows under elevated CO_2 *and warming*

The catchment-scale models demonstrated higher sensitivity and greater year-to-year variability for low flows compared to high flows (Fig. 8). When comparing the annual response in discharge across different years to annual aridity, the models consistently showed higher sensitivity of annual mean and high flows in drier conditions. In contrast, the effect of aridity on low flow sensitivity was less clear.

3.5. Sensitivity of water fluxes at plot versus catchment scale

The annual catchment-averaged climatic water balance, computed as the difference between annual catchment precipitation and potential evapotranspiration, from 1997 to 2016 was 590 ± 165 mm higher than at the plot scale (Fig. 9,a), indicating that the plot scale was considerably more water-limited than the catchment. This difference can be attributed to both lower precipitation amounts and increased actual evapotranspiration (ET_a) at the plot scale (Fig. 9,b), with the latter influenced by its location at a lower elevation compared to the studied catchment. An analysis of groundwater recharge (GWR) sensitivity to aridity shows that both the plot and catchment models are more sensitive during drier years (Fig. 9,c).

4. Discussion

4.1. Sensitivity of the plot-scale model to climate scenarios

In this study, the Penman–Monteith equation and HYDRUS-1D models showed high performance in replicating lysimeter measurements at the plot level, particularly the soil water content and groundwater recharge in the calibration period (2016–2021)(see Supplementary material, Figure S1). Comparing the longer HYDRUS-1D simulation period (1990–2016) with the lysimeter data, the HYDRUS-1D models accurately reflected the sensitivities of actual evapotranspiration and groundwater recharge to ΔCO_2 and ΔT, consistent with the lysimeter dynamics (Fig. 5). While the models demonstrated comparable sensitivity to climate change variables, they exhibited less year-to-year variability compared to the lysimeter measurements. This difference likely arises because models, as simplifications of the natural system, do not fully capture the complex natural variability found in different lysimeter plots across years (Beven, 2011).

4.2. Scaling from plot to catchment: model comparisons and implications

Examining the sensitivity of actual evapotranspiration and groundwater recharge at both plot and catchment scales reveals that at the catchment level, especially in higher elevation areas, actual evapotranspiration shows higher sensitivity. This increase in sensitivity is associated with lower temperatures and higher wind speeds typical of elevated areas. Consequently, shifting from local to catchment scale, particularly in higher elevation areas, leads to a marked increase in actual evapotranspiration sensitivity to ΔT and ΔCO_2. This aligns with findings from prior studies, supporting the hypothesis that altitude-dependent climate conditions can influence evapotranspiration sensitivity (Guo et al., 2017; Sun et al., 2020).

The sensitivity of groundwater recharge to ΔT and ΔCO_2 is less pronounced at the catchment scale. This could be attributed to the higher amount of precipitation the catchment receives (~500 mm $year^{-1}$ greater than plot scale), resulting in more groundwater recharge compared to the plot scale and reduces the impact of potential evapotranspiration. A similar observation was made by other studies (Schübl et al., 2023; Berghuijs et al., 2024), where precipitation dictated the predominant recharge processes. Therefore, at the catchment level, a warmer and more CO_2-enriched future may result in a significant change in actual evapotranspiration (18%–25% for the ΔCT), but the relative change in discharge may be smaller (10%–15% for the ΔCT). On the other hand, at the plot level, even minor relative changes in actual evapotranspiration could have a larger impact on groundwater recharge.

As described in Section 2.4, our study evaluated the impacts of warming on PET under conditions of constant e_a, aligning with our lysimeter experiment setup. We also extended our analysis to include PET changes at constant RH, as recommended for studies analyzing the impacts of global warming by Scheff and Frierson (2014). These additional findings, detailed in the Supplementary material (Figure S8), demonstrated a significantly lower sensitivity to warming compared to our lysimeter observations. This complicates direct comparisons at the plot level, and thus was not included in the main text. Furthermore, the sensitivities computed under constant e_a conditions closely mirrored those reported by other studies in the region. For example, Duethmann and Blöschl (2018) reported similar increases in PET in Austria, observing a 2.8% rise per decade from 1977 to 2014, corresponding to a 0.45 °C temperature increase per decade. This trend suggests a 19% rise in PET with a 3 °C warming—closely reflecting our findings (Fig. 5). Their study, using measured meteorological data including temperature, relative humidity and net radiation, provides a valuable comparison and validates the reliability of our experimental approach. Additionally, our modeled discharge sensitivity aligns with Rhine River discharge projections by Buitink et al. (2021), where a 2.5 °C warming resulted in a 20% reduction in discharge. These similarities indicate that our experimental scenarios were well-aligned with observed regional warming effects. Future research will be better positioned to examine these impacts in more detail when longer time series from lysimeter measurements (Forstner et al., 2021) and eddy covariance data (Pastorello et al., 2020) become available.

When scaling plot findings to the catchment scale, all rainfall–runoff models shared common inputs of rainfall, snowmelt, and PET, and operated on basic groundwater storage assumptions. Despite their differences, the models consistently showed similar patterns in discharge sensitivity and its relationship to water availability. Yet, the sensitivity's magnitude varied, largely due to differing representations of soil water storage and routing mechanisms. These differences affected the calculation of actual evapotranspiration (Fig. 9), impacting both actual evapotranspiration sensitivity, as well as groundwater recharge, and discharge. In line with previous findings (Velázquez et al., 2013; Bastola et al., 2011; Moeck et al., 2016), our findings support the use of multiple models for a more complete evaluation of climate change impacts on water resources, particularly at the catchment level where benchmark data are not available.

These findings highlight the different responses to climate change that emerge when scaling up from plot to catchment level. While these observations may be particularly relevant to mountain catchments like the studied area, where integration across the

whole basin includes inputs from high elevation, high rainfall zones, they also raise important questions about the generalizability of these effects. Further research is needed to understand these dynamics in other types of catchments and under different climatic conditions. This will aid in better predicting the hydrological impacts of climate change and developing effective water resource management strategies for future conditions.

4.3. Increased sensitivity of groundwater recharge and discharge in dry years

In conditions of greater aridity, our study reveals an increased sensitivity of modeled groundwater recharge at both plot and catchment scales, as observed under a future scenario in Fig. 9. The sensitivity becomes more pronounced in drier years, where the reduced total water availability for groundwater recharge or discharge amplifies the response to changes in actual evapotranspiration. However, as opposed to the mean and high flow ($\Delta Q95$), the low flows ($\Delta Q5$) tend to be less sensitive in dry years (low aridity index in Fig. 8). This corresponds to the expectation that the relationship reverses when water availability limits the effect of ΔT on ET, and consequently on GWR and Q. Conversely, under drier conditions with higher temperatures and global radiation, actual evapotranspiration can increase if water availability is not the limiting factor. This phenomenon, known as the drought paradox, leads to amplified decreases in groundwater recharge and river discharge (Mastrotheodoros et al., 2020).

These observations in montane grassland, which are generally energy-limited, highlight the interplay between temperature, evapotranspiration and available water resources, which has important implications for these ecosystems. Shifts in these factors can alter the balance between energy and water availability, leading to shifts in ecosystem dynamics. For example, variations in the annual distribution of precipitation could lead to ecosystems transitioning from energy-limited to water-limited conditions during periods of drought and high temperature (Haslinger et al., 2022; Teuling, 2018), suggesting that future actual evapotranspiration under a warmer climate might be constrained by source limitation (water) or enhanced by source abundance (temperature and radiation).

5. Summary and conclusion

In this study, we investigated how climate change could impact the hydrology of montane grassland. We specifically focused on how sensitive plot and catchment water fluxes were to changes in potential evapotranspiration (PET) due to warming and elevated CO_2 concentrations. To achieve this, we utilized data from a climate change experiment involving lysimeters subjected to warming (ΔT; +3 °C), elevated CO_2 conditions (ΔCO_2; +300 ppm), and a combination of both (ΔCT), to simulate future climate change scenarios. The findings from the lysimeters were modeled using a soil hydrological model and extrapolated to the catchment scale, by employing five different rainfall–runoff models of varying complexity. By adjusting the PET inputs in these models, we were able to simulate changes in actual evapotranspiration (ET_a), as well as the potential impacts of these changes on river discharge (Q) and groundwater recharge (GWR). Our key findings include the following:

1. The soil hydrological models effectively reproduced the lysimeter fluxes-with similar sensitivity to ΔCO_2 and ΔT; however, they exhibited less variation from year-to-year.
2. ΔT increased ET_a and decreased GWR and Q, while ΔCO_2 mitigated the effects of ΔT at both the plot and catchment scale. At the plot scale, ΔCO_2 effects partially buffered the hydrological response of ΔT. Thus, overlooking effects of ΔCO_2 could lead to overestimating the impacts of climate change.
3. The sensitivity of ET_a to ΔT was greater at the catchment than at the plot scale, reflecting increased ET sensitivity to warming with higher elevation. In contrast, GWR was more sensitive at the plot scale, attributed to drier conditions at these lower elevations compared to the catchment scale.
4. Drier conditions increased the sensitivity of GWR and Q to ΔCT across scales, indicating increased risks in a likely future climate.
5. Despite consistent patterns in water flux sensitivity to ΔT and ΔCO_2 across different rainfall–runoff models, variability in impact magnitude underscores the value of multi-model approach for more robust climate change impact assessments on water resources.

CRediT authorship contribution statement

Matevž Vremec: Methodology, Formal analysis, Conceptualization. **Peter Burek:** Writing – review & editing, Methodology. **Luca Guillaumot:** Writing – review & editing, Methodology. **Jesse Radolinski:** Writing – review & editing, Methodology. **Veronika Forstner:** Writing – review & editing, Data curation. **Markus Herndl:** Writing – review & editing, Data curation. **Christine Stumpp:** Writing – review & editing, Methodology. **Michael Bahn:** Writing – review & editing, Methodology. **Steffen Birk:** Writing – review & editing, Methodology, Conceptualization.

Declaration of competing interest

The authors declare that they have no known competing financial interests or personal relationships that could have appeared to influence the work reported in this paper.

Data availability

Data will be made available on request.

Acknowledgments

This work was carried out in the framework of the ClimGrassHydro and RechAUT projects funded by the Austrian Academy of Sciences (ÖAW), and the WaterStressAT project funded by the Austrian Climate Research Programme (ACRP). The lysimeter facility and the project 'Lysi-T-FACE' (DaFNE, 100719) at Gumpenstein was funded by the Austrian Federal Ministry of Agriculture, Forestry, Environment and Water Management (BMLFUW). Meteorological data was provided by the Central Institution for Meteorology and Geodynamics (ZAMG, now Geosphere Austria, Vienna, Austria), Vienna, Austria. We would further thank our colleagues Martina Schink, Andreas Klingler, Andreas Schaumberger, Matthias Kandolf, Medardus Schweiger and Erich Pötsch at the corresponding lysimeter station for their support. The authors acknowledge the financial support by the University of Graz.

Appendix A. Supplementary data

Supplementary material related to this article can be found online at https://doi.org/10.1016/j.ejrh.2024.101970.

References

Aghakouchak, A., Habib, E., 2010. Application of a conceptual hydrologic model in teaching hydrologic processes. pp. 963–973.

Allan, R.P., Barlow, M., Byrne, M.P., Cherchi, A., Douville, H., Fowler, H.J., Gan, T.Y., Pendergrass, A.G., Rosenfeld, D., Swann, A.L.S., Wilcox, L.J., Zolina, O., 2020. Advances in understanding large-scale responses of the water cycle to climate change. Ann. New York Acad. Sci. 1472 (1), 49–75. http://dx.doi.org/10.1111/nyas.14337, URL https://onlinelibrary.wiley.com/doi/10.1111/nyas.14337.

Allen, R.G., Pereira, L.S., Raes, D., Smith, M., et al., 1998. Crop Evapotranspiration-Guidelines for Computing Crop Water Requirements-FAO Irrigation and Drainage Paper 56. Vol. 300, Fao, Rome, p. D05109.

Bastola, S., Murphy, C., Sweeney, J., 2011. The role of hydrological modelling uncertainties in climate change impact assessments of Irish river catchments. Adv. Water Resour. 34 (5), 562–576. http://dx.doi.org/10.1016/j.advwatres.2011.01.008, URL https://linkinghub.elsevier.com/retrieve/pii/S0309170811000224.

Berg, A., Findell, K., Lintner, B., Giannini, A., Seneviratne, S.I., Van Den Hurk, B., Lorenz, R., Pitman, A., Hagemann, S., Meier, A., Cheruy, F., Ducharne, A., Malyshev, S., Milly, P.C.D., 2016. Land–atmosphere feedbacks amplify aridity increase over land under global warming. Nature Clim. Change 6 (9), 869–874. http://dx.doi.org/10.1038/nclimate3029, URL https://www.nature.com/articles/nclimate3029.

Berghuijs, W.R., Collenteur, R.A., Jasechko, S., Jaramillo, F., Luijendijk, E., Moeck, C., Van Der Velde, Y., Allen, S.T., 2024. Groundwater recharge is sensitive to changing long-term aridity. Nature Clim. Change 14 (4), 357–363. http://dx.doi.org/10.1038/s41558-024-01953-z, URL https://www.nature.com/articles/s41558-024-01953-z.

Beven, K.J., 2011. Rainfall-Runoff Modelling: The Primer. John Wiley & Sons.

BMLRT, R., 2020. Grüner Bericht 2020 - Bericht über die situation der österreichischen land- und forstwirtschaft. Technical Report, Bundesminist. Für Nachhalt. Tour., Wien, p. 297 S.

Broderick, C., Matthews, T., Wilby, R.L., Bastola, S., Murphy, C., 2016. Transferability of hydrological models and ensemble averaging methods between contrasting climatic periods: Model transferability. Water Resour. Res. 52 (10), 8343–8373. http://dx.doi.org/10.1002/2016WR018850, URL http://doi.wiley.com/10.1002/2016WR018850.

Buitink, J., Melsen, L.A., Teuling, A.J., 2021. Seasonal discharge response to temperature-driven changes in evaporation and snow processes in the Rhine Basin. Earth Syst. Dyn. 12 (2), 387–400. http://dx.doi.org/10.5194/esd-12-387-2021, URL https://esd.copernicus.org/articles/12/387/2021/.

Burek, P., Satoh, Y., Kahil, T., Tang, T., Greve, P., Smilovic, M., Guillaumot, L., Zhao, F., Wada, Y., 2020. Development of the Community Water Model (CWatM v1.04) – a high-resolution hydrological model for global and regional assessment of integrated water resources management. Geosci. Model Dev. 13 (7), 3267–3298. http://dx.doi.org/10.5194/gmd-13-3267-2020, URL https://gmd.copernicus.org/articles/13/3267/2020/.

Deb, K., Pratap, A., Agarwal, S., Meyarivan, T., 2002. A fast and elitist multiobjective genetic algorithm: NSGA-II. IEEE Trans. Evol. Comput. 6 (2), 182–197. http://dx.doi.org/10.1109/4235.996017, URL http://ieeexplore.ieee.org/document/996017/.

Douville, H., Willett, K.M., 2023. A drier than expected future, supported by near-surface relative humidity observations. Sci. Adv. 9 (30), eade6253. http://dx.doi.org/10.1126/sciadv.ade6253, URL https://www.science.org/doi/10.1126/sciadv.ade6253.

Duethmann, D., Blöschl, G., 2018. Why has catchment evaporation increased in the past 40 years? A data-based study in Austria. Hydrol. Earth Syst. Sci. 22 (10), 5143–5158. http://dx.doi.org/10.5194/hess-22-5143-2018, URL https://hess.copernicus.org/articles/22/5143/2018/.

Duethmann, D., Blöschl, G., Parajka, J., 2020. Why does a conceptual hydrological model fail to correctly predict discharge changes in response to climate change? Hydrol. Earth Syst. Sci. 24 (7), 3493–3511. http://dx.doi.org/10.5194/hess-24-3493-2020, URL https://hess.copernicus.org/articles/24/3493/2020/.

Ernst, P., Loeper, E.G., 1976. Temperaturentwicklung und Vegetationsbeginn auf dem Grunland. Wirtsch. Futter.

Fatichi, S., Pappas, C., Ivanov, V.Y., 2016. Modeling plant–water interactions: an ecohydrological overview from the cell to the global scale. WIREs Water 3 (3), 327–368. http://dx.doi.org/10.1002/wat2.1125, URL https://onlinelibrary.wiley.com/doi/10.1002/wat2.1125.

Forstner, V., Groh, J., Vremec, M., Herndl, M., Vereecken, H., Gerke, H.H., Birk, S., Pütz, T., 2021. Response of water fluxes and biomass production to climate change in permanent grassland soil ecosystems. Hydrol. Earth Syst. Sci. 25 (12), 6087–6106. http://dx.doi.org/10.5194/hess-25-6087-2021, URL https://hess.copernicus.org/articles/25/6087/2021/.

Forstner, V., Vremec, M., Herndl, M., Birk, S., 2023. Effects of dry spells on soil moisture and yield anomalies at a montane managed grassland site: A lysimeter climate experiment. Ecohydrology http://dx.doi.org/10.1002/eco.2518, URL https://onlinelibrary.wiley.com/doi/10.1002/eco.2518.

Fortin, F.A., De Rainville, F.M., Gardner, M., Parizeau, M., Gagńe, C., 2012. DEAP: Evolutionary Algorithms Made Easy. Vol. 13, pp. 2171–2175.

Gauch, M., Kratzert, F., Gilon, O., Gupta, H., Mai, J., Nearing, G., Tolson, B., Hochreiter, S., Klotz, D., 2023. In defense of metrics: Metrics sufficiently encode typical human preferences regarding hydrological model performance. Water Resour. Res. 59 (6), e2022WR033918. http://dx.doi.org/10.1029/2022WR033918, URL https://agupubs.onlinelibrary.wiley.com/doi/10.1029/2022WR033918.

Green, T.R., Taniguchi, M., Kooi, H., Gurdak, J.J., Allen, D.M., Hiscock, K.M., Treidel, H., Aureli, A., 2011. Beneath the surface of global change: Impacts of climate change on groundwater. J. Hydrol. 405 (3–4), 532–560. http://dx.doi.org/10.1016/j.jhydrol.2011.05.002, URL https://linkinghub.elsevier.com/retrieve/pii/S0022169411002988.

Guo, D., Westra, S., Maier, H.R., 2017. Sensitivity of potential evapotranspiration to changes in climate variables for different Australian climatic zones. Hydrol. Earth Syst. Sci. 21 (4), 2107–2126. http://dx.doi.org/10.5194/hess-21-2107-2017, URL https://hess.copernicus.org/articles/21/2107/2017/.

Hanus, S., Hrachowitz, M., Zekollari, H., Schoups, G., Vizcaino, M., Kaitna, R., 2021. Future changes in annual, seasonal and monthly runoff signatures in contrasting Alpine catchments in Austria. Hydrol. Earth Syst. Sci. 25 (6), 3429–3453. http://dx.doi.org/10.5194/hess-25-3429-2021, URL https://hess.copernicus.org/articles/25/3429/2021/.

Haslinger, K., Schöner, W., Abermann, J., Laaha, G., Andre, K., Olefs, M., Koch, R., 2022. Contradictory Signal in Future Surface Water Availability in Austria: Increase on Average Vs. Higher Probability of Droughts. preprint, Atmospheric, Meteorological and Climatological Hazards, http://dx.doi.org/10.5194/egusphere-2022-191, URL https://egusphere.copernicus.org/preprints/2022/egusphere-2022-191/.

Herndl, M., Pötsch, E., Bohner, A., Kandolf, M., 2011. Lysimeter als Bestandteil eines technischen Versuchskonzeptes zur Simulation der Erderwärmung im Grünland. In: Bericht LFZ Raumberg- Gumpenstein, 14. Gumpensteiner Lysimetertagung "Lysimeter in Der Klimafolgenforschung". ISBN-13: 978-3-902559-61-6. pp. 119–126.

Hiebl, J., Frei, C., 2016. Daily temperature grids for Austria since 1961—concept, creation and applicability. Theor. Appl. Climatol. 124 (1), 161–178. http://dx.doi.org/10.1007/s00704-015-1411-4, Publisher: Springer.

Hiebl, J., Frei, C., 2018. Daily precipitation grids for Austria since 1961—development and evaluation of a spatial dataset for hydroclimatic monitoring and modelling. Theor. Appl. Climatol. 132 (1–2), 327–345. http://dx.doi.org/10.1007/s00704-017-2093-x, URL https://link.springer.com/10.1007/s00704-017-2093-x.

Houska, T., Kraft, P., Chamorro-Chavez, A., Breuer, L., 2015. SPOTting model parameters using a ready-made python package. PLoS One 10, 1–22. http://dx.doi.org/10.1371/journal.pone.0145180, Publisher: Public Library of Science.

Inauen, N., Körner, C., Hiltbrunner, E., 2013. Hydrological consequences of declining land use and elevated CO_2 in alpine grassland. In: Bardgett, R. (Ed.), J. Ecol. 101 (1), 86–96. http://dx.doi.org/10.1111/1365-2745.12029, URL https://onlinelibrary.wiley.com/doi/10.1111/1365-2745.12029.

IPCC, 2021. The physical science basis. Contribution of Working Group I to the sixth assessment report of the intergovernmental panel on climate change. In: Climate Change 2021. Cambridge University Press.

Karlsson, I.B., Sonnenborg, T.O., Refsgaard, J.C., Trolle, D., Børgesen, C.D., Olesen, J.E., Jeppesen, E., Jensen, K.H., 2016. Combined effects of climate models, hydrological model structures and land use scenarios on hydrological impacts of climate change. J. Hydrol. 535, 301–317. http://dx.doi.org/10.1016/j.jhydrol.2016.01.069, URL https://linkinghub.elsevier.com/retrieve/pii/S0022169416300099.

Kimball, B.A., 2005. Theory and performance of an infrared heater for ecosystem warming. Global Change Biol. 11 (11), 2041–2056. http://dx.doi.org/10.1111/j.1365-2486.2005.1028.x, URL https://onlinelibrary.wiley.com/doi/10.1111/j.1365-2486.2005.1028.x.

Kling, H., Fuchs, M., Paulin, M., 2012. Runoff conditions in the upper Danube basin under an ensemble of climate change scenarios. J. Hydrol. 424–425, 264–277. http://dx.doi.org/10.1016/j.jhydrol.2012.01.011, URL https://linkinghub.elsevier.com/retrieve/pii/S0022169412000431.

Leakey, A.D.B., Ainsworth, E.A., Bernacchi, C.J., Rogers, A., Long, S.P., Ort, D.R., 2009. Elevated CO2 effects on plant carbon, nitrogen, and water relations: six important lessons from FACE. J. Exp. Botany 60 (10), 2859–2876. http://dx.doi.org/10.1093/jxb/erp096, URL https://academic.oup.com/jxb/article-lookup/doi/10.1093/jxb/erp096.

Liu, Y., Fernández-Ortega, J., Mudarra, M., Hartmann, A., 2022. Pitfalls and a feasible solution for using KGE as an informal likelihood function in MCMC methods: $DREAM_{(ZS)}$ as an example. Hydrol. Earth Syst. Sci. 26 (20), 5341–5355. http://dx.doi.org/10.5194/hess-26-5341-2022, URL https://hess.copernicus.org/articles/26/5341/2022/.

Mastrotheodoros, T., Pappas, C., Molnar, P., Burlando, P., Manoli, G., Parajka, J., Rigon, R., Szeles, B., Bottazzi, M., Hadjidoukas, P., Fatichi, S., 2020. More green and less blue water in the Alps during warmer summers. Nature Clim. Change 10 (2), 155–161. http://dx.doi.org/10.1038/s41558-019-0676-5, URL http://www.nature.com/articles/s41558-019-0676-5.

Miglietta, F., Hoosbeek, M.R., Foot, J., Gigon, F., Hassinen, A., Heijmans, M., Peressotti, A., Saarinen, T., van Breemen, N., Wallén, B., 2001. Spatial and temporal performance of the MiniFACE (free air CO2 enrichment) system on bog ecosystems in Northern and central Europe. Environ. Monit. Assess. 66 (2), 107–127. http://dx.doi.org/10.1023/A:1026495830251.

Milly, P.C.D., Dunne, K.A., 2016. Potential evapotranspiration and continental drying. Nature Clim. Change 6, http://dx.doi.org/10.1038/nclimate3046.

Moeck, C., Brunner, P., Hunkeler, D., 2016. The influence of model structure on groundwater recharge rates in climate-change impact studies. Hydrogeol. J. 24 (5), 1171–1184. http://dx.doi.org/10.1007/s10040-016-1367-1, URL http://link.springer.com/10.1007/s10040-016-1367-1.

Moore, R.J., 1985. The probability-distributed principle and runoff production at point and basin scales. Hydrol. Sci. J. 30 (2), 273–297. http://dx.doi.org/10.1080/02626668509490989, URL http://www.tandfonline.com/doi/abs/10.1080/02626668509490989.

Pastorello, G., Trotta, C., Canfora, E., Chu, H., Christianson, D., Cheah, Y.-W., Poindexter, C., Chen, J., Elbashandy, A., Humphrey, M., Isaac, P., Polidori, D., Reichstein, M., Ribeca, A., van Ingen, C., Vuichard, N., Zhang, L., Amiro, B., Ammann, C., Arain, M.A., Ardö, J., Arkebauer, T., Arndt, S.K., Arriga, N., Aubinet, M., Aurela, M., Baldocchi, D., Barr, A., Beamesderfer, E., Marchesini, L.B., Bergeron, O., Beringer, J., Bernhofer, C., Berveiller, D., Billesbach, D., Black, T.A., Blanken, P.D., Bohrer, G., Boike, J., Bolstad, P.V., Bonal, D., Bonnefond, J.-M., Bowling, D.R., Bracho, R., Brodeur, J., Brümmer, C., Buchmann, N., Burban, B., Burns, S.P., Buysse, P., Cale, P., Cavagna, M., Cellier, P., Chen, S., Chini, I., Christensen, T.R., Cleverly, J., Collalti, A., Consalvo, C., Cook, B.D., Cook, D., Coursolle, C., Cremonese, E., Curtis, P.S., D'Andrea, E., da Rocha, H., Dai, X., Davis, K.J., Cinti, B.D., Grandcourt, A.d., Ligne, A.D., De Oliveira, R.C., Delpierre, N., Desai, A.R., Di Bella, C.M., Tommasi, P.d., Dolman, H., Domingo, F., Dong, G., Dore, S., Duce, P., Dufrêne, E., Dunn, A., Dušek, J., Eamus, D., Eichelmann, U., ElKhidir, H.A.M., Eugster, W., Ewenz, C.M., Ewers, B., Famulari, D., Fares, S., Feigenwinter, I., Feitz, A., Fensholt, R., Filippa, G., Fischer, M., Frank, J., Galvagno, M., Gharun, M., Gianelle, D., Gielen, B., Gioli, B., Gitelson, A., Goded, I., Goeckede, M., Goldstein, A.H., Gough, C.M., Goulden, M.L., Graf, A., Griebel, A., Gruening, C., Grünwald, T., Hammerle, A., Han, S., Han, X., Hansen, B.U., Hanson, C., Hatakka, J., He, Y., Hehn, M., Heinesch, B., Hinko-Najera, N., Hörtnagl, L., Hutley, L., Ibrom, A., Ikawa, H., Jackowicz-Korczynski, M., Janouš, D., Jans, W., Jassal, R., Jiang, S., Kato, T., Khomik, M., Klatt, J., Knohl, A., Knox, S., Kobayashi, H., Koerber, G., Kolle, O., Kosugi, Y., Kotani, A., Kowalski, A., Kruijt, B., Kurbatova, J., Kutsch, W.L., Kwon, H., Launiainen, S., Laurila, T., Law, B., Leuning, R., Li, Y., Liddell, M., Limousin, J.-M., Lion, M., Liska, A.J., Lohila, A., López-Ballesteros, A., López-Blanco, E., Loubet, B., Loustau, D., Lucas-Moffat, A., Lüers, J., Ma, S., Macfarlane, C., Magliulo, V., Maier, R., Mammarella, I., Manca, G., Marcolla, B., Margolis, H.A., Marras, S., Massman, W., Mastepanov, M., Matamala, R., Matthes, J.H., Mazzenga, F., McCaughey, H., McHugh, I., McMillan, A.M.S., Merbold, L., Meyer, W., Meyers, T., Miller, S.D., Minerbi, S., Moderow, U., Monson, R.K., Montagnani, L., Moore, C.E., Moors, E., Moreaux, V., Moureaux, C., Munger, J.W., Nakai, T., Neirynck, J., Nesic, Z., Nicolini, G., Noormets, A., Northwood, M., Nosetto, M., Nouvellon, Y., Novick, K., Oechel, W., Olesen, J.E., Ourcival, J.-M., Papuga, S.A., Parmentier, F.-J., Paul-Limoges, E., Pavelka, M., Peichl, M., Pendall, E., Phillips, R.P., Pilegaard, K., Pirk, N., Posse, G., Powell, T., Prasse, H., Prober, S.M., Rambal, S., Rannik, U., Raz-Yaseef, N., Rebmann, C., Reed, D., Dios, V.R.d., Restrepo-Coupe, N., Reverter, B.R., Roland, M., Sabbatini, S., Sachs, T., Saleska, S.R., Sánchez-Cañete, E.P., Sanchez-Mejia, Z.M., Schmid, H.P., Schmidt, M., Schneider, K., Schrader, F., Schroder, I., Scott, R.L., Sedlák, P., Serrano-Ortíz, P., Shao, C., Shi, P., Shironya, I., Siebicke, L., Šigut, L., Silberstein, R., Sirca, C., Spano, D., Steinbrecher, R., Stevens, R.M., Sturtevant, C., Suyker, A., Tagesson, T., Takanashi, S., Tang, Y., Tapper, N., Thom, J., Tomassucci, M., Tuovinen, J.-P., Urbanski, S., Valentini, R., van der Molen, M., van Gorsel, E., van Huissteden, K., Varlagin, A., Verfaillie, J., Vesala, T., Vincke, C., Vitale, D., Vygodskaya, N., Walker, J.P., Walter-Shea, E., Wang, H., Weber, R., Westermann, S., Wille, C., Wofsy, S., Wohlfahrt, G., Wolf, S., Woodgate, W., Li, Y., Zampedri, R., Zhang, J., Zhou, G., Zona, D., Agarwal, D., Biraud, S., Torn, M., Papale, D., 2020. The FLUXNET2015 dataset and the ONEFlux processing pipeline for eddy covariance data. Sci. Data 7 (1), 225. http://dx.doi.org/10.1038/s41597-020-0534-3, URL https://www.nature.com/articles/s41597-020-0534-3.

Perrin, C., Michel, C., Andréassian, V., 2003. Improvement of a parsimonious model for streamflow simulation. J. Hydrol. 279 (1–4), 275–289. http://dx.doi.org/10.1016/S0022-1694(03)00225-7, URL https://linkinghub.elsevier.com/retrieve/pii/S0022169403002257.

Piepho, H.-P., Herndl, M., Pötsch, E.M., Bahn, M., 2017. Designing an experiment with quantitative treatment factors to study the effects of climate change. J. Agron. Crop Sci. 203 (6), 584–592. http://dx.doi.org/10.1111/jac.12225, URL https://onlinelibrary.wiley.com/doi/10.1111/jac.12225.

Ritchie, J.T., 1972. Model for predicting evaporation from a row crop with incomplete cover. Water Resour. Res. 8 (5), 1204–1213. http://dx.doi.org/10.1029/WR008i005p01204, URL http://doi.wiley.com/10.1029/WR008i005p01204.

Schaumberger, A., 2011. Räumliche Modelle zur Vegetations-und Ertragsdynamik im Wirtschaftsgrünland. Dissertation.

Scheff, J., Frierson, D.M.W., 2014. Scaling potential evapotranspiration with greenhouse warming. J. Clim. 27 (4), 1539–1558. http://dx.doi.org/10.1175/JCLI-D-13-00233.1, URL http://journals.ametsoc.org/doi/10.1175/JCLI-D-13-00233.1.

Schübl, M., Brunetti, G., Fuchs, G., Stumpp, C., 2023. Estimating vadose zone water fluxes from soil water monitoring data: a comprehensive field study in Austria. Hydrol. Earth Syst. Sci. 27 (7), 1431–1455. http://dx.doi.org/10.5194/hess-27-1431-2023, URL https://hess.copernicus.org/articles/27/1431/2023/.

Schübl, M., Stumpp, C., Brunetti, G., 2022. A Bayesian perspective on the information content of soil water measurements for the hydrological characterization of the vadose zone. J. Hydrol. 613, 128429. http://dx.doi.org/10.1016/j.jhydrol.2022.128429, URL https://linkinghub.elsevier.com/retrieve/pii/S0022169422009994.

Shen, H., Tolson, B.A., Mai, J., 2022. Time to update the split-sample approach in hydrological model calibration. Water Resour. Res. 58 (3), http://dx.doi.org/10.1029/2021WR031523, URL https://onlinelibrary.wiley.com/doi/10.1029/2021WR031523.

Shepherd, T.G., 2019. Storyline approach to the construction of regional climate change information. Proc. R. Soc. A 475 (2225), 20190013. http://dx.doi.org/10.1098/rspa.2019.0013, URL https://royalsocietypublishing.org/doi/10.1098/rspa.2019.0013.

Šimůnek, J., Van Genuchten, M.T., Šejna, M., 2008. Development and applications of the hydrus and stanmod software packages and related codes. Vadose Zone J. 7 (2), 587–600. http://dx.doi.org/10.2136/vzj2007.0077, URL https://acsess.onlinelibrary.wiley.com/doi/10.2136/vzj2007.0077.

Stumpp, C., Stichler, W., Kandolf, M., Šimůnek, J., 2012. Effects of land cover and fertilization method on water flow and solute transport in five lysimeters: A long-term study using stable water isotopes. Vadose Zone J. 11 (1), http://dx.doi.org/10.2136/vzj2011.0075, URL http://doi.wiley.com/10.2136/vzj2011.0075.

Sun, J., Wang, G., Sun, X., Lin, S., Hu, Z., Huang, K., 2020. Elevation-dependent changes in reference evapotranspiration due to climate change. Hydrol. Process. 34 (26), 5580–5594. http://dx.doi.org/10.1002/hyp.13978, URL https://onlinelibrary.wiley.com/doi/10.1002/hyp.13978.

Teuling, A.J., 2018. A hot future for European droughts. Nature Clim. Change 8 (5), 364–365. http://dx.doi.org/10.1038/s41558-018-0154-5, URL http://www.nature.com/articles/s41558-018-0154-5.

Ukkola, A.M., Prentice, I.C., Keenan, T.F., Van Dijk, A.I.J.M., Viney, N.R., Myneni, R.B., Bi, J., 2016. Reduced streamflow in water-stressed climates consistent with CO2 effects on vegetation. Nature Clim. Change 6 (1), 75–78. http://dx.doi.org/10.1038/nclimate2831, URL http://www.nature.com/articles/nclimate2831.

Van Genuchten, M.T., 1980. A closed-form equation for predicting the hydraulic conductivity of unsaturated soils. Soil Sci. Soc. Am. J. 44 (5), 892–898. http://dx.doi.org/10.2136/sssaj1980.03615995004400050002x, URL http://doi.wiley.com/10.2136/sssaj1980.03615995004400050002x.

Van Tiel, M., Weiler, M., Freudiger, D., Moretti, G., Kohn, I., Gerlinger, K., Stahl, K., 2023. Melting alpine water towers aggravate downstream low flows: A stress-test storyline approach. Earth's Future 11 (3), e2022EF003408. http://dx.doi.org/10.1029/2022EF003408, URL https://agupubs.onlinelibrary.wiley.com/doi/10.1029/2022EF003408.

Van Vuuren, D.P., Edmonds, J., Kainuma, M., Riahi, K., Thomson, A., Hibbard, K., Hurtt, G.C., Kram, T., Krey, V., Lamarque, J.-F., et al., 2011. The representative concentration pathways: an overview. Clim. Change 109 (1), 5–31. http://dx.doi.org/10.1007/s10584-011-0148-z, Publisher: Springer.

Velázquez, J.A., Schmid, J., Ricard, S., Muerth, M.J., Gauvin St-Denis, B., Minville, M., Chaumont, D., Caya, D., Ludwig, R., Turcotte, R., 2013. An ensemble approach to assess hydrological models' contribution to uncertainties in the analysis of climate change impact on water resources. Hydrol. Earth Syst. Sci. 17 (2), 565–578. http://dx.doi.org/10.5194/hess-17-565-2013, URL https://hess.copernicus.org/articles/17/565/2013/.

Virtanen, P., Gommers, R., Oliphant, T.E., Haberland, M., Reddy, T., Cournapeau, D., Burovski, E., Peterson, P., Weckesser, W., Bright, J., van der Walt, S.J., Brett, M., Wilson, J., Millman, K.J., Mayorov, N., Nelson, A.R.J., Jones, E., Kern, R., Larson, E., Carey, C.J., Polat, I., Feng, Y., Moore, E.W., VanderPlas, J., Laxalde, D., Perktold, J., Cimrman, R., Henriksen, I., Quintero, E.A., Harris, C.R., Archibald, A.M., Ribeiro, A.H., Pedregosa, F., van Mulbregt, P., SciPy 1.0 Contributors, 2020. SciPy 1.0: Fundamental algorithms for scientific computing in Python. Nature Methods 17, 261–272. http://dx.doi.org/10.1038/s41592-019-0686-2.

Vremec, M., Collenteur, R., Birk, S., 2024. PyEt v1.3.1: a Python package for the estimation of potential evapotranspiration. http://dx.doi.org/10.5194/gmd-2024-63, URL https://gmd.copernicus.org/preprints/gmd-2024-63/.

Vremec, M., Forstner, V., Herndl, M., Collenteur, R., Schaumberger, A., Birk, S., 2023. Sensitivity of evapotranspiration and seepage to elevated atmospheric CO 2 from lysimeter experiments in a montane grassland. J. Hydrol. 617, 128875. http://dx.doi.org/10.1016/j.jhydrol.2022.128875, URL https://linkinghub.elsevier.com/retrieve/pii/S0022169422014457.

Vremec, M., Klingler, A., Herndl, M., Schaumberger, A., Birk, S., 2021. Estimating crop evapotranspiration of managed alpine grassland using remotely sensed LAI.

Vrugt, J.A., 2016. Markov chain Monte Carlo simulation using the DREAM software package: Theory, concepts, and MATLAB implementation. Environ. Model. Softw. 75, 273–316. http://dx.doi.org/10.1016/j.envsoft.2015.08.013, URL https://linkinghub.elsevier.com/retrieve/pii/S1364815215300396.

Wagner, T., Themeßl, M., Schüppel, A., Gobiet, A., Stigler, H., Birk, S., 2017. Impacts of climate change on stream flow and hydro power generation in the Alpine region. Environ. Earth Sci. 76 (1), 4. http://dx.doi.org/10.1007/s12665-016-6318-6.

Ward, E.J., Oren, R., Seok Kim, H., Kim, D., Tor-ngern, P., Ewers, B.E., McCarthy, H.R., Oishi, A.C., Pataki, D.E., Palmroth, S., Phillips, N.G., Schäfer, K.V.R., 2018. Evapotranspiration and water yield of a pine-broadleaf forest are not altered by long-term atmospheric [CO $_2$] enrichment under native or enhanced soil fertility. Global Change Biol. 24 (10), 4841–4856. http://dx.doi.org/10.1111/gcb.14363, URL https://onlinelibrary.wiley.com/doi/10.1111/gcb.14363.

Wieser, G., Hammerle, A., Wohlfahrt, G., 2008. The water balance of grassland ecosystems in the Austrian alps. Arct. Antarct. Alp. Res. 40 (2), 439–445. http://dx.doi.org/10.1657/1523-0430(07-039)[WIESER]2.0.CO;2, URL https://ww.tandfonline.com/doi/full/10.1657/1523-0430(07-039)[WIESER]2.0.CO;2.

Yang, Y., McVicar, T.R., Yang, D., Zhang, Y., Piao, S., Peng, S., Beck, H.E., 2021. Low and contrasting impacts of vegetation CO₂ fertilization on global terrestrial runoff over 1982–2010: accounting for aboveground and belowground vegetation–CO₂ effects. Hydrol. Earth Syst. Sci. 25 (6), 3411–3427. http://dx.doi.org/10.5194/hess-25-3411-2021, URL https://hess.copernicus.org/articles/25/3411/2021/.

Yang, Y., Roderick, M.L., Zhang, S., McVicar, T.R., Donohue, R.J., 2019. Hydrologic implications of vegetation response to elevated CO2 in climate projections. Nature Clim. Change 9 (1), 44–48. http://dx.doi.org/10.1038/s41558-018-0361-0, URL https://www.nature.com/articles/s41558-018-0361-0.

Zhang, Y., Zheng, H., Zhang, X., Leung, L.R., Liu, C., Zheng, C., Guo, Y., Chiew, F.H.S., Post, D., Kong, D., Beck, H.E., Li, C., Blöschl, G., 2023. Future global streamflow declines are probably more severe than previously estimated. Nat. Water 1 (3), 261–271. http://dx.doi.org/10.1038/s44221-023-00030-7, URL https://www.nature.com/articles/s44221-023-00030-7.